

Phase diagram and optical conductivity of the ionic Hubbard model

Ph. Brune ^a, G. I. Japaridze ^{a,b}, and A. P. Kampf ^a

^a *Institut für Physik, Theoretische Physik III, Elektronische Korrelationen und Magnetismus, Universität Augsburg, 86135 Augsburg, Germany*

^b *Institute of Physics, Georgian Academy of Sciences, Guramishvili Str. 6, 380077, Tbilisi, Georgia*

We investigate the ground state phase diagram of the one-dimensional “ionic” Hubbard model with an alternating periodic potential at half filling by the bosonization technique as well as by numerical diagonalization of finite systems with the Lanczos and DMRG methods. Our results support the existence of a single “metallic” transition point from a band to a Mott insulator. In addition, we present results for the optical conductivity obtained by the recently developed dynamical DMRG method. The band insulator to Mott insulator phase transition is discussed in detail including a critical review of existing approaches and results for the ionic Hubbard model.

PACS numbers: 71.10.-w, 71.10.Fd, 71.10.Hf, 71.27.+a, 71.30.+h

I. INTRODUCTION

For more than two decades the correlation induced metal-insulator (MI) transition and its characteristics has been one of the challenging problems in condensed matter physics [1]. As a function of the electronic coupling strength this MI transition is often accompanied with a symmetry breaking and the development of long range order [2]. In dimension $D=1$ in particular this ordering can only be connected to the breaking of a discrete symmetry. Examples include commensurate charge density waves, Peierls phenomena with dimerization patterns which may occur even in the absence of an electron-lattice coupling due to electronic interactions only. The MI transition can be driven either by varying the electron density or the electron-electron interaction strength. If the MI transition is approached from the metallic side the electrical conductivity or the electronic compressibility may be used to characterize the transition; the approach of the MI transition from the insulating side may on the other hand be properly captured by the divergent behavior of the electric susceptibility [3].

In addition, also the features of the insulating phase may qualitatively change with the interaction strength allowing for quantum phase transitions between insulating phases, i.e. insulator-insulator transitions. The extended Hubbard model at half-filling with an on-site (U) and a nearest neighbor (V) Coulomb repulsion provides a prominent example with a transition from a Mott insulator to a charge density wave insulator in the vicinity of the line $U = 2V$ in the phase diagram [4]. In recent years another example for an extension of the Hubbard model has received special attention which includes a staggered potential term [6–8]. The corresponding Hamiltonian has been named “ionic Hubbard model”; at half-filling this model undergoes a different kind of an insulator-insulator transition from a band to a Mott insulator which we investigate in detail in this work using both, numerical and analytical tools in 1D. Specifically we study the Hamiltonian

$$H = -t \sum_{i,\sigma} (1 + (-1)^i \delta) (c_{i\sigma}^\dagger c_{i+1\sigma} + h.c.) + U \sum_i n_{i\uparrow} n_{i\downarrow} + \frac{\Delta}{2} \sum_i (-1)^i n_i, \quad (1)$$

where $c_{i\sigma}^\dagger$ creates an electron on site i with spin σ , $n_{i\sigma} = c_{i\sigma}^\dagger c_{i\sigma}$, t is the nearest-neighbor hopping amplitude, U the on-site Hubbard interaction, Δ the potential energy difference between neighboring sites on a chain, and δ an additional Peierls modulation of the hopping matrix element t .

In the limit $\Delta = \delta = 0$ Eq. (1) reduces to the ordinary *Hubbard model*, the limit $\Delta = 0$ and $\delta > 0$ is called the *Peierls-Hubbard model*, and the limit $\Delta > 0$ and $\delta = 0$ usually is referred to as the *ionic Hubbard model*. In the following, we will focus mainly on the effect of the on-site modulation Δ , so we implicitly assume $\delta = 0$ except where stated otherwise.

Our results support the previously anticipated [8] existence of a single transition at a critical coupling $U_C(\Delta)$ from a band insulator with equal spin and charge excitation gaps to a Mott insulating phase with a vanishing spin gap. The transition is first order and results from a ground state level crossing with a change of the parity eigenvalue of the ground state wave function. Furthermore, we provide the first numerical evaluation of the optical conductivity for the ionic Hubbard model which allows for an additional characterization of the “metallic” transition point $U_C(\Delta)$ where the charge gap closes.

The outline of our paper is as follows: In chapter II we describe the original physical motivation for the ionic Hubbard model which was first studied in the context of phenomena in 1D charge transfer salts. In chapter III–V we summarize previously proposed scenarios for the ground state phase diagram using bosonization and symmetry arguments, respectively, as well as a strong coupling expansion. Chapter VI contains a detailed reanalysis of the bosonization approach to the ionic Hubbard model. In chapters VII and VIII we present our numerical Lanczos and density matrix renormalization

group (DMRG) results from which we draw conclusions for the ground state phase diagram, and in chapter IX we discuss dynamical DMRG results for the optical conductivity. Finally, we conclude and summarize our results in chapter X.

II. NEUTRAL-IONIC TRANSITION

The “ionic” Hubbard model was first proposed and discussed almost 20 years ago in the context of organic mixed stack charge transfer crystals consisting of a sequence of alternating donor (D) and acceptor (A) molecules ($\dots D^{+\rho}A^{-\rho}D^{+\rho}A^{-\rho}\dots$) [5,6]. These stacks form quasi 1D insulating or semiconducting chains and are classified into two categories depending on the amount of charge transfer ρ : quasi-neutral for $\rho < 0.5$, and quasi-ionic for $\rho > 0.5$. Torrance *et al.* [5] found that at room temperature and pressure, these materials are either mostly ionic ($\rho \approx 1$) or mostly neutral ($\rho \approx 0$), but that several of these systems undergo a reversible neutral to ionic phase transition (NIT), i.e. a discontinuous jump in the ionicity ρ upon changing temperature or pressure.

The prototype system for this NIT is tetrathiafulvalene (TTF)- p -chloranil (hereafter TTF-CA), with TTF as the donor and p -chloranil as the acceptor molecule [5]. In this system, at ambient pressure the NIT takes place at a critical temperature $T_C \approx 81\text{K}$, connected with a sharp jump of ρ , and a simultaneous dimeric displacement of the D - A molecular units, i.e. a Peierls distortion of the $D - A$ chains [9,10]. In addition, a NIT with by a discontinuous jump in ρ takes also place at a critical pressure $p_C \approx 11\text{kbar}$ at room temperature. The existence of the NIT results from the competition between the effective ionization energy of a D - A pair, controlled by the electron affinities of the A and D molecules, and the long-range electrostatic Madelung energy gained by the ionized lattice.

The NIT in TTF-CA at finite temperatures has been intensively studied theoretically in a series of articles by Nagaosa *et al.* [6] using quantum Monte Carlo simulations. As a model for TTF-CA, Nagaosa *et al.* [6] used the 1D ionic Hubbard model (1) with $\Delta > 0$ and $\delta = 0$ at half filling. This model serves as an appropriate effective model for a D - A chain, with the even sites representing the LUMO (Lowest Unoccupied Molecular Orbital) of an acceptor molecule, while the odd sites represent the HOMO (Highest Occupied Molecular Orbital) of a donor. In the neutral state, these orbitals would be occupied by either no or two electrons, respectively. The model parameters U and Δ in (1) were used for an effective description of the microscopic parameters [11]. Within this picture, Δ could be interpreted as the energy necessary to move an electron from the donor to the acceptor.

In addition, the ionic Hubbard model has been used to describe the ferroelectric transition in perovskite materials such as BaTiO_3 [12–14] (or KNbO_3 [17]). The ori-

gin of ferroelectricity was usually discussed in the past in terms of ionic displacements and the internal Lorentz field produced by the polarization. However, this simple view may be inadequate due to the covalent nature of the Ti-O bond, which was demonstrated by LDA calculations [15], and experiments, where the actual valence of Ti was measured to be $+2.9$ [16]. Thus, even though the formal valence of Ti is $4+$ with a d^0 configuration in the purely ionic picture, the actual valence of Ti is less than $3+$ with a d^1 configuration due to dp hybridization. The ionic Hubbard model here is used as a simple model for a binary compound, AB , with the A sites (i even) representing the transition metal element (Ti), and the B sites (i odd) representing the oxygen. The on-site energy modulation Δ in this case is the relative difference of the energy levels on the A (Ti) and B (O) sites, i.e. $\Delta = E_A - E_B$ [12,13].

In the “modern” theory of spontaneous ferroelectric polarization, it has been shown that polarization is really related to the quantum mechanical many-body wavefunction of the electrons (instead of the local charge density), and can be formulated in terms of a Berry’s phase (or Zak’s phase [18]) involving integrals over the phases of the wavefunction [19]. Within this framework, the polarization in ferroelectric perovskites has been studied within an LDA calculation for KNbO_3 [19], and by exact diagonalization and Hartree-Fock analysis of the ionic Hubbard model (1) [14,20,21].

III. INSULATOR-INSULATOR TRANSITION

For an understanding of the existence of a phase transition in the ionic Hubbard model with $\delta = 0$ the best starting point is the atomic limit, following an argument by Gidopoulos *et al.* [8]. For $t = 0$, it is immediately seen that for half filling and $U < \Delta$ the ground state of (1) has two electrons on the B (i odd), and no electrons on the A sites (i even) (“neutral” phase). This corresponds to a charge density wave (CDW) ordering with maximum amplitude. On the other hand, for $U > \Delta$ each site is occupied by one electron (“ionic” phase). Obviously, for $t = 0$ a transition occurs at a critical value $U_C = \Delta$. This transition at a finite critical value $U_C > 0$ is expected to persist for finite hopping matrix elements $t > 0$, where the alternating potential still defines two sublattices A and B , doubling the unit cell and opening up a band gap Δ for $U = 0$ at $k = \pm\pi/2$. For $t > 0$ the critical coupling shifts to $U_C(t) > \Delta$, with U_C monotonically increasing with increasing Δ . For $U, \Delta \gg t$ the system is close to the atomic limit, and U_C approaches Δ from above.

For $U = 0$ the ground state of the model at half-filling is a CDW band insulator, its elementary excitation spectrum consists of particle-hole excitations over the band gap. We consider a system to be in a band insulator (BI) phase when the criterion $\Delta_S = \Delta_C$ holds, where the spin (Δ_S) and the charge gap (Δ_C) are given by

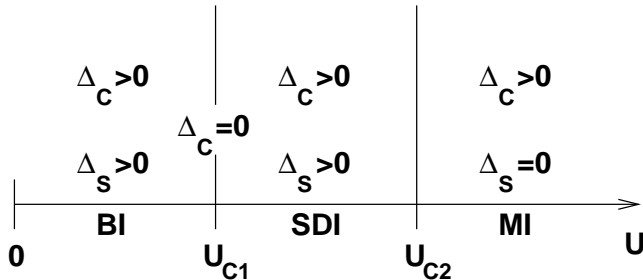


FIG. 1. Schematic ground state phase diagram of the ionic Hubbard model for a fixed ionic potential $\Delta > 0$ at half-filling as obtained from the bosonization approach of Ref. [7]. BI, SDI, and MI denote band-, spontaneously dimerized, and Mott insulating phases, respectively.

$$\begin{aligned}
 \Delta_S &= E_0(N = L, S_z = 1) - E_0(N = L, S_z = 0) \\
 \Delta_C &= E_0(N = L + 1, S_z = 1/2) \\
 &\quad + E_0(N = L - 1, S_z = 1/2) \\
 &\quad - 2E_0(N = L, S_z = 0) \quad .
 \end{aligned} \tag{2}$$

$E_0(N, S_z)$ is the ground state energy, L the system length, N the number of electrons in the system, and S_z the z -component of the total spin. On the other hand, in the “ionic phase” for $U > U_C$, e.g. when $U \gg t, \Delta$, the charge gap is set by the Coulomb interaction U , thus the system is a correlated insulator with $\Delta_C > \Delta_S$. However, in contrast to the cases with $\Delta = 0$ or $t = 0$, the CDW order is present in this phase for all finite values of U , i.e. except for $U \rightarrow +\infty$. If also $\Delta_S = 0$, i.e. if the system is a true Mott insulator (MI) in the ionic phase, or $\Delta_S > 0$, is an important question closely related to the physics of the intermediate region around $U \approx \Delta$, as well as the nature of the phase transition from the band to the correlated or Mott insulator.

Thus, the ionic Hubbard model is different from the Peierls-Hubbard model ($\delta > 0, \Delta = 0$), which is also a BI at $U = 0$, but in contrast to the ionic Hubbard model there is $\Delta_C > \Delta_S > 0$ for any value $U > 0$, i.e. the phase transition from the Peierls band insulator to the correlated insulator occurs at $U_C = 0$.

Recently, renewed interest in the ionic Hubbard model started with the field theoretical bosonization analysis of Fabrizio, Gogolin and Nersesyan (FGN) [7], and numerical exact diagonalization studies [8], where a new scenario for the intermediate region $U \approx \Delta$ was proposed. Several subsequent numerical treatments of the model [22–25] lead to partially contradicting results. The main differences are the nature of the insulator-insulator phase transition, the possible existence of a metallic point with $\Delta_C = 0$ at a critical U_C , and the question whether the spin gap closes for $U > U_C$.

FGN derived a schematic phase diagram within the framework of bosonization techniques as reproduced in Fig. 1. The authors of Ref. [7] argue that for small but finite U the BI persists up to a critical value U_{C1} where

$\Delta_C = 0$, and the system might be “metallic”. Upon further increasing U they predicted a “spontaneously dimerized” insulating (SDI) (or bond order wave (BOW)) intermediate phase, which should undergo a continuous transition into the correlated (or Mott) insulating phase at a second critical value $U_{C2} > U_{C1}$. Such a dimerized or BOW ground state would be characterized by long range staggered bond-bond correlations

$$g_B(r) = \frac{1}{L} \sum_i \langle \psi_0 | B_i B_{i+r} | \psi_0 \rangle \quad , \tag{3}$$

$$B_i = \sum_{\sigma} \left(c_{i\sigma}^{\dagger} c_{i+1\sigma} + h.c. \right) \quad . \tag{4}$$

FGN argue that such a state would also imply a finite spin gap $\Delta_S > 0$. The basic calculational steps and the sequence of arguments and assumptions of the bosonization technique will be summarized in chapter VI.

Such a SDI state has been recently claimed to be observed numerically by Wilkens and Martin [24] in a variational quantum Monte Carlo study. More precisely, the authors of Ref. [24] observed one transition from the BI to the correlated SDI phase, but no second transition to the MI. Recent DMRG results [23] support the existence of only one transition point at U_C , at which $\Delta_C = 0$, and the system undergoes a direct transition from a band to a Mott insulator. Qin *et al.* [23] conclude from finite size extrapolations that $\Delta_S = 0$ above the transition, in agreement with the results of previous exact diagonalization studies [14,20].

IV. SYMMETRY ANALYSIS

Valuable insight into the nature of the BI-MI transition is obtained from a symmetry analysis. The Hamiltonian (1) is invariant with respect to *inversion* at a site i and *translation* by two lattice sites. Thus, there exists a common eigenbasis of the Hamiltonian and these two symmetry operations, i.e. any nondegenerate eigenstate of H is also an eigenstate of the operators that generate the corresponding symmetry transformation. If we denote the site inversion operator by P , defined through

$$P c_{i\sigma}^{\dagger} P^{\dagger} = c_{L-i\sigma}^{\dagger} \quad \text{for } i = 0, 1, \dots, L-1 \tag{5}$$

$$P|0\rangle = |0\rangle \quad , \tag{6}$$

with $|0\rangle$ being the electron vacuum state, and \hat{T}_j for a translation by j sites, then any nondegenerate eigenstate $|\psi_n\rangle$ of H must obey $P|\psi_n\rangle = \pm|\psi_n\rangle$ (due to $P^2 = 1$) and $\hat{T}_2|\psi_n\rangle = |\psi_n\rangle$. Because of $[H, \hat{T}_1] \neq 0$, a non-degenerate eigenstate $|\psi_n\rangle$ of H can not be an eigenstate of \hat{T}_1 . This suggests that an alternating charge order in the ground state at $U = 0$ will persist up to $U \rightarrow +\infty$, with just the amplitude of the density modulation decreasing with increasing U .

For the half-filled Hubbard model ($\Delta = \delta = 0$) the parity eigenvalue of the ground state for site inversion can be determined in the limits $U = 0$ and $U \gg t$ [8]. For $U = 0$, the ground state is a direct product of spin up and spin down Slater determinants, both formed from the same occupied spatial wavefunctions having the same parity $P_\sigma = \pm 1$, so the parity eigenvalue of the total wavefunction is given by their product

$$P = P_\downarrow \times P_\uparrow = 1 \quad (7)$$

for the two spin projections. Hence, the state at $U = 0$ is even under site inversion. On the other hand, in the large U limit ($U \gg t$) the mapping to the Heisenberg Hamiltonian can be used to show that for a finite number of lattice sites $L = 4n$ with periodic boundary conditions (PBC) or $L = 4n + 2$ with antiperiodic boundary conditions (APBC) the ground state obeys $P|\psi_0\rangle = -|\psi_0\rangle$ (for details see [8]). In finite chains, these combinations of chain lengths and boundary conditions correspond to a choice of the distribution of the allowed momenta k in the Brillouin zone (BZ) such that $k = \pi/2$ is an allowed k value. This is important at half filling, where $k = \pi/2$ is the BZ boundary. It follows, that upon increasing the number of sites L , the ground state for $U \gg t$ will be odd with respect to P as long as $k = \pi/2$ is an allowed k value, and this feature will therefore persist in the thermodynamic limit $L \rightarrow +\infty$. This implies that for the ordinary Hubbard model the discrete inversion symmetry changes between $U = 0$ and $U \gg t$. Since the model does not show a phase transition for $U > 0$, the ground state has $P = +1$ only for $U = 0$, and $P = -1$ for any $U > 0$.

However, in the ionic Hubbard model ($\Delta > 0$) the phase transition from a BI to a correlated insulator occurs at some finite $U_C > 0$. This suggests that the parity of the ground state remains even not only for $U = 0$, but for all $U < U_C$. At U_C , a ground state level crossing occurs, as confirmed by exact diagonalization studies (see below), connected with a site parity change of the ground state. Above U_C the ground state has odd site parity (as the ordinary Hubbard model), and the system continuously approaches its limiting behavior described by an effective spin model as $U \rightarrow \infty$.

V. STRONG COUPLING EXPANSION

In the strong coupling limit, the ionic Hubbard model was argued in previous treatments (except Ref. [24]) to be a MI with $\Delta_S = 0$. For the Hamiltonian (1) with $\delta = 0$ and $U \gg t, \Delta$ the effective Heisenberg spin model [6]

$$H_{eff} = J \sum_i \left(\mathbf{S}_i \cdot \mathbf{S}_{i+1} - \frac{1}{4} \right) + J' \sum_i \left(\mathbf{S}_i \cdot \mathbf{S}_{i+2} - \frac{1}{4} \right) \quad (8)$$

was derived to describe the low-energy physics. In Eq. (8) the exchange couplings are given by

$$J = \frac{4t^2}{U} \left[\frac{1}{1-x^2} - \frac{4t^2}{U^2} \frac{1+4x^2-x^4}{(1-x^2)^3} \right],$$

$$J' = \frac{4t^4}{U^3} \frac{(1+4x^2-x^4)}{(1-x^2)^3}, \quad (9)$$

where $x = \Delta/U$, which we have independently rederived following the method of MacDonald *et al.* [26]. In the derivation the Hilbert space of the ionic Hubbard model is split up into two subspaces — one that contains no doubly occupied sites, and one that contains all states with at least one or more doubly occupied sites. The atomic limit ($t = 0$) of the ionic Hubbard model (1) is taken as the unperturbed problem H_0 , and the kinetic term in (1) is treated as a perturbation. The ground state of H_0 is therefore in the subspace without double occupancies, which is infinitely degenerate due to the spin degrees of freedom. The kinetic term lifts the degeneracy in this subspace. Introducing the projection operator $P = \prod_i (1 - n_{i\uparrow} n_{i\downarrow})$, the effective Hamiltonian $H_{eff} = P \exp(iS) H \exp(-iS) P$ is obtained by expanding (1) in powers of t/U around H_0 , using a canonical transformation S that renders H independent of terms connecting subspaces with different numbers of double occupancies up to a given order in t/U [26,27].

The result (8) implies that for the ionic Hubbard model ($\Delta > 0$) in the strong coupling limit the low-energy physics is qualitatively similar to that of the ordinary Hubbard model ($\Delta = 0$), with modified exchange coupling constants J and J' . For next-nearest neighbor couplings $J' < 0.24J$ the spin gap vanishes [28]; thus the system would be a MI. The coupling constants (9) fulfill $J' < 0.24J$ at least for $U > 3.6t$ for $\Delta \leq t$ and $U > 3.6\Delta$ for $\Delta > t$. Since the t/U expansion is valid only for $U \gg t, \Delta$, this would imply that the ionic Hubbard model is indeed a MI ($\Delta_S = 0$) in the strong coupling limit. However, the effective model (8) is invariant with respect to translations by *one* lattice spacing, whereas the original ionic Hubbard model is invariant only with respect to translations by *two* lattice spacings. Thus, the effective spin Hamiltonian has a higher symmetry than the original model it was derived from and the arguments of the strong coupling expansion in favour of $\Delta_S = 0$ for $U > U_C$ cannot be considered rigorous.

In Ref. [6] the authors showed that the higher translational symmetry of the spin model will remain up to infinite order in the expansion in t/U . But, since $\Delta > 0$ in the ionic Hubbard model manifestly leads to a staggered charge density, any approach based on projecting out completely the double occupancy does not respect the symmetry of the Hamiltonian.

Of course, also in the Hubbard chain for any non-infinite U the double occupancy is not zero. However, this 'virtual doublons' are equally distributed over all sites therefore do not change the translational symme-

try. If only the spin excitations are considered, these doublons are never traced. The same is expected to hold also for the ionic Hubbard model in the large U limit; its spin channel should look the same as the spin channel of the ordinary Hubbard model. The peculiarity of the ionic Hubbard model is thus hidden in the charge sector.

In numerical DMRG and exact diagonalization calculations a finite charge modulation due to $\Delta > 0$ is observed for arbitrarily large but finite values of U , which is reasonable, because $[H, \hat{T}_1] \neq 0$, and a ground state obeying $\hat{T}_1|\psi_0\rangle = |\psi_0\rangle$ then would have a higher symmetry than the Hamiltonian itself. Thus, we conclude that the alternating charge ordering structure of the ground state at $U = 0$ will persist up to $U \rightarrow +\infty$, and since the ground state of the effective Heisenberg spin model obeys $\hat{T}_1|\psi_0\rangle = |\psi_0\rangle$, the spin model alone cannot describe all the essential features of the ionic Hubbard model even at large U .

VI. BOSONIZATION RESULTS

In this section we analyse the ionic Hubbard Hamiltonian (1) (with $\delta = 0$) using the continuum-limit bosonization approach. As indicated above, the model was recently studied within the same approach by Fabrizio, Gogolin and Nersisyan [7]. Below we mainly follow the route by FGN, and highlight the important issues partially in preparation of the discussion of our numerical data presented in subsequent chapters.

In what follows we derive the low-energy effective field theory of the lattice model (1). Considering the weak-coupling case $U, \Delta \ll t$ we linearize the spectrum and pass to the continuum limit by use of the mapping:

$$a_0^{-1/2} c_{n,\sigma} \rightarrow i^n R_\sigma(x) + (-i)^n L_\sigma(x). \quad (10)$$

Here $x = na_0$, a_0 is the lattice spacing, and $R_\sigma(x)$ and $L_\sigma(x)$ describe right-moving and left-moving particles, respectively. These fields can be bosonized in a standard way [29]:

$$R_\sigma(x) = (2\pi a_0)^{-1/2} e^{i\sqrt{4\pi}\Phi_{R,\sigma}(x)}, \quad (11)$$

$$L_\sigma(x) = (2\pi a_0)^{-1/2} e^{-i\sqrt{4\pi}\Phi_{L,\sigma}(x)}, \quad (12)$$

where $\Phi_{R,(L);\sigma}(x)$ are the right (left) moving Bose fields. We introduce the field $\Phi_\sigma(x) = \Phi_{R,\sigma}(x) + \Phi_{L,\sigma}(x)$ and obtain the following bosonized version of the model (1)

$$\mathcal{H} = \mathcal{H}_\uparrow + \mathcal{H}_\downarrow + \mathcal{H}_{\uparrow\downarrow} \quad , \quad (13)$$

$$\mathcal{H}_\sigma = \int dx \left\{ \frac{v_F}{2} [P_\sigma^2(x) + (\partial_x \Phi_\sigma)^2] \right. \quad (14)$$

$$\left. - \frac{\Delta}{2\pi a} \sin(\sqrt{4\pi}\Phi_\sigma) \right\} \quad , \quad (15)$$

$$\mathcal{H}_{\uparrow\downarrow} = U \int dx \left\{ \frac{1}{\pi} (\partial_x \Phi_\uparrow)(\partial_x \Phi_\downarrow) \right. \quad (16)$$

$$\left. + \frac{1}{\pi^2 a_0^2} \sin(\sqrt{4\pi}\Phi_\uparrow) \sin(\sqrt{4\pi}\Phi_\downarrow) \right\} \quad .$$

Here $P_\sigma(x)$ is the momentum conjugate to $\Phi_{R,\sigma}(x)$.

Introducing the linear combinations

$$\phi_c = \frac{1}{\sqrt{2}}(\Phi_\uparrow + \Phi_\downarrow), \quad \phi_s = \frac{1}{\sqrt{2}}(\Phi_\uparrow - \Phi_\downarrow) \quad (17)$$

to describe the charge (ϕ_c) and spin (ϕ_s) degrees of freedom, respectively, and after rescaling of these fields we rewrite the bosonized Hamiltonian in the following way:

$$\mathcal{H} = \mathcal{H}_c + \mathcal{H}_s + \mathcal{H}_{cs} \quad , \quad (18)$$

$$\mathcal{H}_c = \int dx \left\{ \frac{v_c}{2} [P_c^2(x) + (\partial_x \phi_c)^2] \right. \quad (19)$$

$$\left. - \frac{U}{2\pi\alpha_0^2} \cos(\sqrt{8\pi K_c} \phi_c(x)) \right\} \quad ,$$

$$\mathcal{H}_s = \int dx \left\{ \frac{v_s}{2} [P_s^2(x) + (\partial_x \phi_s)^2] \right. \quad (20)$$

$$\left. + \frac{U}{2\pi\alpha_0^2} \cos(\sqrt{8\pi} \phi_s(x)) \right\} \quad ,$$

$$\mathcal{H}_{cs} = -\frac{\Delta}{\pi a_0} \int dx \sin(\sqrt{2\pi K_c} \phi_c) \cos(\sqrt{2\pi} \phi_s). \quad (21)$$

A. Symmetries

As we outlined in chapter IV a symmetry analysis is an important tool towards understanding the phase diagram and the insulator-insulator transition in the ionic Hubbard model. We therefore consider first the symmetry aspects of the bosonized Hamiltonian. The three generators of the spin- $SU(2)$ algebra

$$S^+ = \sum_n c_{n,\uparrow}^\dagger c_{n,\downarrow}, \quad S^- = \sum_n c_{n,\downarrow}^\dagger c_{n,\uparrow},$$

$$S^z = \sum_n \frac{1}{2} (c_{n,\uparrow}^\dagger c_{n,\uparrow} - c_{n,\downarrow}^\dagger c_{n,\downarrow}), \quad (22)$$

commute with the Hamiltonian (1) which shows its $SU(2)$ -spin invariance. The electron-hole transformation

$$c_{n,\sigma} \rightarrow (-1)^n c_{n,\sigma}^\dagger \quad (23)$$

$$R_\sigma \rightarrow R_\sigma^\dagger, \quad L_\sigma \rightarrow L_\sigma^\dagger$$

$$\Phi_\sigma \rightarrow -\Phi_\sigma, \quad \phi_{c,s} \rightarrow -\phi_{c,s}$$

converts $\mathcal{H}\{U, \Delta\} \rightarrow \mathcal{H}\{U, -\Delta\}$ and is not the symmetry operation at $\Delta \neq 0$. The transformation

$$c_{n,\uparrow} \rightarrow c_{n,\uparrow}^\dagger, \quad c_{n,\downarrow} \rightarrow (-1)^n c_{n,\downarrow}^\dagger, \quad (24)$$

$$R_\uparrow (L_\uparrow) \rightarrow R_\uparrow (L_\uparrow)^\dagger, \quad R_\downarrow \rightarrow R_\downarrow^\dagger, \quad L_\downarrow \rightarrow L_\downarrow^\dagger$$

$$\Phi_\uparrow \rightarrow \Phi_\uparrow, \quad \Phi_\downarrow \rightarrow -\Phi_\downarrow$$

$$\phi_c \rightarrow \phi_s, \quad \phi_s \rightarrow \phi_c,$$

is not the symmetry operation of the model either, since it maps the repulsive $U > 0$ (attractive $U < 0$) ionic-Hubbard model into the ordinary Hubbard model with

attractive (repulsive) interaction in the presence of an alternating magnetic field. Therefore, contrary to the half-filled Hubbard model where the charge sector is governed by the same $SU(2)$ symmetry as the spin sector, the charge sector of the ionic-Hubbard model exhibits only $U(1)$ -symmetry.

Next we consider the set of discrete symmetries for a chain of length L with periodic boundary conditions. The translation operation by m lattice sites \hat{T}_m .

$$\begin{aligned} \hat{T}_m c_{n,\sigma} &\rightarrow c_{n+m,\sigma} & (25) \\ R_\sigma &\rightarrow i^m R_\sigma, & L_s \rightarrow (-i)^m L_s \\ \Phi_\sigma &\rightarrow \Phi_\sigma + m\sqrt{\pi}/2, \\ \phi_c &\rightarrow \phi_c + m\sqrt{\pi/2}, & \phi_s \rightarrow \phi_s \end{aligned}$$

converts $\mathcal{H}\{U, \Delta\} \rightarrow \mathcal{H}\{U, (-1)^m \Delta\}$ and is not a symmetry operation of the model for $m = 2k + 1$.

The site parity operation \hat{P}_s , i.e. the inversion operation around the site 0 as described by the set of transformations

$$\begin{aligned} c_{n,\sigma} &\rightarrow c_{L-n,\sigma} & (26) \\ R_\sigma &\rightarrow L_\sigma, & L_s \rightarrow R_s \\ \Phi_\sigma &\rightarrow -\Phi_\sigma + \sqrt{\pi}/2, \\ \phi_c &\rightarrow -\phi_c, & \phi_s \rightarrow -\phi_s + \sqrt{\pi/2} \end{aligned}$$

is indeed the symmetry operation of the ionic-Hubbard Hamiltonian as anticipated and explained before.

The link parity \hat{P}_l i.e. the inversion operation around the link 0, 1 with the mapping

$$\begin{aligned} c_{n,\sigma} &\rightarrow c_{L-n+1,\sigma} & (27) \\ R_\sigma &\rightarrow iL_\sigma, & L_s \rightarrow -iR_s \\ \Phi_\sigma &\rightarrow -\Phi_\sigma, \\ \phi_c &\rightarrow -\phi_c, & \phi_s \rightarrow -\phi_s, \end{aligned}$$

however, is not a symmetry operation of the model.

We note that the transformations (23)-(27) leave the operators $\cos(\sqrt{8\pi}\phi_c)$ and $\cos(\sqrt{8\pi}\phi_s)$ invariant. The bosonized version of the ordinary Hubbard model ($\Delta = 0$) is given only in terms of these operators and derivatives of the fields, which proves the $SU(2) \otimes SU(2)$, electron-hole, translational, site and link inversion invariance of the Hubbard Hamiltonian. As we observe the ionic distortion makes the charge sector $U(1)$ -symmetric and violates the translational symmetry by one lattice unit as well as the link-inversion symmetry.

B. Topological Excitations

We first recall the results for the noninteracting case. At $U = 0$ the Hamiltonian (13) is a direct sum of two sine-Gordon (SG) models with the coupling constant $\beta = \sqrt{4\pi}$. Each SG model describes free massive fermions with the spin projections $\sigma = \pm 1/2$. These massive

fermions are identified as the quantum solitons of the $\beta^2 = 4\pi$ SG model. The quantum soliton corresponds to a configuration of the field ϕ_σ connecting two neighboring minima of the $\sin(\sqrt{4\pi}\phi_\sigma)$ potential

$$\begin{aligned} \phi_\sigma(x = -\infty) &= 0, \\ \phi_\sigma(x = +\infty) &= \sqrt{\pi} \end{aligned} \quad . \quad (28)$$

Such an excitation carries the charge $N_\sigma = \pm 1$ with the fermion numbers N_σ defined by

$$N_\sigma = \frac{1}{\sqrt{\pi}} \int_{-\infty}^{\infty} dx \partial_x \phi_\sigma(x) \quad . \quad (29)$$

The total charge and the total spin carried by massive spinful fermions are defined as

$$Q = N_\uparrow + N_\downarrow, \quad S_z = \frac{N_\uparrow - N_\downarrow}{2} \quad . \quad (30)$$

The simplest excitation is obtained by considering a soliton (antisoliton), e.g. in the spin- \uparrow component, keeping the vacuum state intact for the spin- \downarrow component: $N_\uparrow = \pm 1$, $N_\downarrow = 0$. Such a state has the total charge $Q = \pm 1$ and the total spin $S_z = \pm 1/2$. This leads to the conclusion that free massive fermions are the elementary excitations of the model in the band insulating phase, each carrying the unit charge and spin $1/2$.

We can similarly examine the $U = 0$ case by using the equivalent bosonized version (18). Since the potential

$$V(\phi_c, \phi_s) \sim -\Delta \cdot \sin(\sqrt{2\pi}\phi_c) \cos(\sqrt{2\pi}\phi_s) \quad (31)$$

represents a strongly relevant perturbation (with scaling dimension 1), the groundstate of the model is described by a strong coupling regime with the fields ϕ_c and ϕ_s locked at some values.

The locations of the degenerate vacua of this potential are given by its extrema, obtained from

$$\cos(\sqrt{2\pi}\phi_c) \cos(\sqrt{2\pi}\phi_s) = 0, \quad (32)$$

$$\sin(\sqrt{2\pi}\phi_c) \sin(\sqrt{2\pi}\phi_s) = 0 \quad . \quad (33)$$

Since the spin-rotational $SU(2)$ symmetry cannot be broken, it follows that $\sin(\sqrt{2\pi}\phi_s) = 0$. This yields

$$\sqrt{2\pi}\phi_s = \pi \cdot n \quad (n \in \mathbb{Z}) \quad . \quad (34)$$

Since $\cos\phi_s \neq 0$, it follows $\cos(\sqrt{2\pi}\phi_c) = 0$ and

$$\sqrt{2\pi}\phi_c = \frac{\pi}{2} + \pi \cdot m \quad (m \in \mathbb{Z}) \quad . \quad (35)$$

Thus, for $\Delta > 0$, the vacua of the potential (21) fall into two sets:

$$\sqrt{2\pi}\phi_s = 2n \cdot \pi, \quad \sqrt{2\pi}\phi_c = \frac{\pi}{2} + 2m \cdot \pi \quad (36)$$

$$\sqrt{2\pi}\phi_s = (2n + 1) \cdot \pi, \quad \sqrt{2\pi}\phi_c = -\frac{\pi}{2} + 2m \cdot \pi \quad . \quad (37)$$

In order to build up *single-particle* excitations, one has to take into account “inter-set” transitions connecting the vacua from the two different sets. Consider e.g. a transition from

$$\begin{aligned}\phi_s = 0 &\rightarrow \phi_s = \sqrt{\frac{\pi}{2}} \\ \phi_c = \sqrt{\frac{\pi}{8}} &\rightarrow \phi_c = -\sqrt{\frac{\pi}{8}}.\end{aligned}\quad (38)$$

The spin and charge quantum numbers associated with these topological excitations are given by

$$Q = \sqrt{\frac{2}{\pi}} \int_{-\infty}^{\infty} dx \partial_x \phi_c(x) = -1 \quad , \quad (39)$$

$$S_z = \frac{1}{\sqrt{2\pi}} \int_{-\infty}^{\infty} dx \partial_x \phi_s(x) = 1/2 \quad , \quad (40)$$

corresponding to those of a single massive fermion, which is the elementary excitation in the BI.

To build up pure *charge* or *spin* excitations one has to consider “intra-set” transitions. Consider, for instance, the situation when we lock the charge at $\phi_c = \sqrt{\pi/8}$ and consider a spin soliton connecting the states $\phi_s = 0$ and $\phi_s = \sqrt{2\pi}$. Such a soliton carries the spin $S = 1$ and charge $Q = 0$. Similarly, if we lock the spin, e.g. at $\phi_s = 0$, and consider a charge soliton interpolating between $\phi_c = \sqrt{\pi/8}$ and $\phi_c = \sqrt{\pi/8} + \sqrt{2\pi}$, the soliton will carry the charge $Q = 2$ and spin $S_z = 0$.

Let us now recall the results for the half-filled Hubbard model. At $\Delta = 0$ the Hamiltonian (18) is a direct sum of two SG models with a marginal value of the coupling constant $\beta = \sqrt{8\pi}$ describing the charge and spin degrees of freedom, respectively. At $U > 0$ the backscattering contribution ($U \cos(\sqrt{8\pi}\phi_s)$) to the spin sector is marginally irrelevant and therefore can be neglected. For this reason the spin sector is gapless and the field ϕ_s remains disordered. However, the umklapp term is relevant, the charge sector is gapped and the field ϕ_c is locked in minima of the potential $-U \cos(\sqrt{8\pi}\phi_c)$, i.e.

$$\sqrt{2\pi}\phi_c = \pi \cdot m \quad (m \in \mathbb{Z}) \quad . \quad (41)$$

From (39) it is clear that the elementary topological excitation corresponding to transition between two nearest minima will carry the charge $Q = 1$ and spin $S_z = 0$. Notice, however, that the positions of the vacua in (41) are different from those in the case $U = 0$ (35). This means that the crossover between the Mott-Hubbard and the BI phase should be associated with a significant redistribution of the charge density of the system.

C. Forward scattering model with ionic and/or Peierls distortion

To get more insight into the details of the physics of the ionic-Hubbard model, we first restrict ourselves to the

limit of a weak Hubbard interaction $U \ll \Delta \ll t$, where the properties of the system are mostly determined by the strong ionic distortion. In the infrared (low energy - large distance) limit the umklapp and backward scattering processes, described in Eq. (18) by $U \cos(\sqrt{8\pi K_c \phi_c(x)})$ and $U \cos(\sqrt{8\pi} \phi_s(x))$ terms, respectively, are frozen out. Therefore, we initially neglect these terms and consider the Hamiltonian

$$\begin{aligned}\mathcal{H}_{TL} = &\int dx \left\{ \frac{v_c}{2} [P_c^2(x) + (\partial_x \phi_c)^2] \right\} \\ &+ \int dx \left\{ \frac{v_s}{2} [P_s^2(x) + (\partial_x \phi_s)^2] \right\} \\ &- \frac{\Delta}{\pi a_0} \int dx \sin(\sqrt{2\pi K_c \phi_c}) \cos(\sqrt{2\pi K_s \phi_s}) \quad ,\end{aligned}\quad (42)$$

i.e. the half-filled Tomonaga-Luttinger model with ionic distortion. The noninteracting electron system corresponds to the particular limit $K_c = K_s = 1$. For generality we do not assume the $SU(2)$ symmetry of the spin channel and therefore the parameter K_s is not obligatorily equal to unity. In context of the initial ionic-Hubbard model at this stage we focus our studies on effects arising from the effective long-distance part of the electron-electron interaction.

Let us decouple the interaction term in a mean-field manner introducing

$$m_c = \Delta \cdot \langle \cos(\sqrt{2\pi K_s \phi_s}) \rangle \quad , \quad (43)$$

$$m_s = \Delta \cdot \langle \sin(\sqrt{2\pi K_c \phi_c}) \rangle \quad . \quad (44)$$

The mean-field version of the bosonized Hamiltonian then reads

$$\mathcal{H} = \mathcal{H}_c + \mathcal{H}_s \quad , \quad (45)$$

$$\begin{aligned}\mathcal{H}_c = &\int dx \left\{ \frac{v_c}{2} [P_c^2(x) + (\partial_x \phi_c)^2] \right. \\ &\left. - \frac{m_c}{\pi a_0} \sin(\sqrt{2\pi K_c \phi_c}) \right\},\end{aligned}\quad (46)$$

$$\begin{aligned}\mathcal{H}_s = &\int dx \left\{ \frac{v_s}{2} [P_s^2(x) + (\partial_x \phi_s)^2] \right. \\ &\left. - \frac{m_s}{\pi a_0} \cos(\sqrt{2\pi K_s \phi_s}) \right\}.\end{aligned}\quad (47)$$

Since we are in the massive phase of the SG model ($K_{c,s} \simeq 1$) we can estimate the renormalized masses as

$$M_c \simeq \Lambda \left(\frac{m_c}{\Lambda} \right)^{2/(4-K_c)} \quad , \quad (48)$$

$$M_s \simeq \Lambda \left(\frac{m_s}{\Lambda} \right)^{2/(2-K_s)} \quad , \quad (49)$$

where Λ - is the cut-off energy. Similarly, the expectation values of $\sin(\sqrt{2\pi K_c \phi_c})$ and $\cos(\sqrt{2\pi K_s \phi_s})$ are estimated as

$$\langle \sin(\sqrt{2\pi K_c \phi_c}) \rangle \simeq \left(\frac{m_c}{\Lambda} \right)^{K_c/(4-K_c)} \quad (50)$$

$$\langle \cos(\sqrt{2\pi K_s \phi_s}) \rangle \simeq \left(\frac{m_s}{\Lambda} \right)^{K_s/(4-K_s)} \quad . \quad (51)$$

The self-consistency equation

$$\Delta = \frac{m_c}{\langle \sin(\sqrt{2\pi K_s} \phi_s) \rangle} = \frac{m_s}{\langle \sin(\sqrt{2\pi K_c} \phi_c) \rangle} \quad (52)$$

leads to

$$\frac{m_s}{\Lambda} = \left(\frac{m_c}{\Lambda} \right)^{(4-K_s)/(4-K_c)}. \quad (53)$$

Using Eqs. (43)-(52) one easily finds that

$$M_s = M_c = \Lambda \left(\frac{\Delta}{\Lambda} \right)^{2/(4-K_c-K_s)}$$

and the system shows the properties of the BI with a weakly renormalized value of the excitation gap. In particular, for the non-interacting system $K_c = K_s = 1$ and $M_s = M_c = \Delta$.

It is rather instructive to compare the ionic Hubbard model with the Peierls-Hubbard model. The bosonized expression for the Peierls distortion term is given by

$$-\frac{\delta}{\pi a_0} \cos(\sqrt{2\pi} \phi_c) \cos(\sqrt{2\pi} \phi_s). \quad (54)$$

By following again the steps of the above performed analysis it is straightforward to show that the half-filled Tomonaga-Luttinger model with Peierls distortion exhibits the properties of the BI with equal charge and spin gaps.

D. Renormalization effects from the short distance interaction

In order to account for the renormalization of the BI gap by the short-distance part of the interaction we consider again the limiting case $U \ll \Delta \ll t$. In this limit we treat both, the ionic term and the Hubbard interaction on the same footing in a perturbative way.

For this purpose it is convenient to consider the two-dimensional Euclidean action of the model:

$$\begin{aligned} S &= S_0 + S_{int}, \\ S_0 &= v_F \int d^2 \mathbf{x} \left\{ \frac{1}{2} [(\nabla \phi_c)^2 + (\nabla \phi_s)^2] \right\}, \\ S_{int} &= v_F \int d^2 \mathbf{x} \left\{ \frac{m_{cs}}{\pi a_0} \sin(\sqrt{2\pi K_c} \phi_c) \cos(\sqrt{2\pi} \phi_s) \right. \\ &\quad \left. + \frac{M_c}{\pi a_0^2} \cos(\sqrt{8\pi K_c} \phi_c) + \frac{M_s}{\pi a_0^2} \cos(\sqrt{8\pi} \phi_s) \right\}. \end{aligned} \quad (55)$$

Here, the dimensionless coupling constants are given by:

$$M_c = -\frac{U}{4\pi t}, \quad M_s = \frac{U}{4\pi t}, \quad m_{cs} = -\frac{\Delta}{2\pi t}. \quad (56)$$

Expanding the partition function to the second order

$$\begin{aligned} Z &= \int D\Phi_s D\Phi_c e^{-S[\Phi_c, \Phi_s]} \\ &= \int D\Phi_s D\Phi_c e^{-S_0[\Phi_c, \Phi_s]} [1 - S_{int} + \frac{1}{2} S_{int}^2 + \dots] \end{aligned} \quad (57)$$

we integrate out all configurations in the second order term with $|\mathbf{x} - \mathbf{x}'| \sim a_0$. Using the following operator product expansion formulas:

$$\begin{aligned} \int \frac{d^2 \mathbf{x}}{a_0^2} \int \frac{d^2 \mathbf{x}'}{a_0^2} \sin(\phi(\mathbf{x})) \cdot \cos(2\phi(\mathbf{x}')) &= \\ -\frac{\pi}{2} \int \frac{d^2 \mathbf{x}}{a_0^2} [\sin(\phi_c(\mathbf{x})) + \dots], \end{aligned} \quad (58)$$

$$\begin{aligned} \int \frac{d^2 \mathbf{x}}{a_0^2} \int \frac{d^2 \mathbf{x}'}{a_0^2} \cos(\phi(\mathbf{x})) \cdot \cos(2\phi(\mathbf{x}')) &= \\ +\frac{\pi}{2} \int \frac{d^2 \mathbf{x}}{\pi a_0^2} [\cos(\phi_c(\mathbf{x})) + \dots], \end{aligned} \quad (59)$$

$$\begin{aligned} \int \frac{d^2 \mathbf{x}}{a_0^2} \int \frac{d^2 \mathbf{x}'}{a_0^2} \cos(\phi(\mathbf{x})) \cdot \cos(\phi(\mathbf{x}')) &= \\ +\frac{\pi}{2} \int \frac{d^2 \mathbf{x}}{a_0^2} [1 - \frac{1}{2} (\nabla \phi_c)^2 + \cos(2\phi(\mathbf{x})) + \dots], \end{aligned} \quad (60)$$

$$\begin{aligned} \int \frac{d^2 \mathbf{x}}{a_0^2} \int \frac{d^2 \mathbf{x}'}{a_0^2} \sin(\phi(\mathbf{x})) \cdot \sin(\phi(\mathbf{x}')) &= \\ +\frac{\pi}{2} \int \frac{d^2 \mathbf{x}}{a_0^2} [1 - \frac{1}{2} (\nabla \phi_c)^2 - \cos(2\phi(\mathbf{x})) + \dots], \end{aligned} \quad (61)$$

where dots denote strongly irrelevant terms of higher critical dimensionality, we obtain the following renormalization of the model parameters:

$$\tilde{\Delta} = \Delta \left(1 - \lambda_1 \frac{U}{t} \right), \quad (62)$$

$$\tilde{M}_c = -U \left(1 - \lambda_2 \frac{\Delta^2}{Ut} \right), \quad (63)$$

$$\tilde{M}_s = U \left(1 - \lambda_2 \frac{\Delta^2}{Ut} \right). \quad (64)$$

Here, $\lambda_{i=1,2,3}$ are numbers of order unity. As we observe, at $U > 0$ amplitudes of the umklapp and backward scattering processes (M_c and M_s , respectively) reduce quadratically, while the parameter of the ionic distortion is renormalized linearly by the on-site repulsion. Therefore, at $U \ll \Delta \ll t$ the system displays the properties of the band insulator with a linearly in U decreasing gap. The $U \leftrightarrow -U$ asymmetry of the model is also clearly seen: at $U > 0$ the amplitude of the strongly relevant umklapp scattering (M_c) decreases, while at $U < 0$ the amplitude of the strongly relevant backscattering processes (M_c) increases. Thus, we conclude that the BI phase is more stable against the Hubbard interaction for the repulsive interaction than in the case of an attractive on-site coupling.

In the case of a Peierls distortion the effect of the electron-electron interaction at short distances is rather

different. Assuming $U \ll \delta \ll t$ the same procedure which for the ionic model leads to the linear in U renormalization of the gap in the BI phase Eqs. (63)-(64), gives for the Peierls-Hubbard model the following expressions for the renormalized parameters

$$\tilde{\delta} = \delta \left(1 + O\left(\frac{U}{t}\right)^2 \right), \quad (65)$$

$$\tilde{M}_c^P = -U \left(1 + \lambda'_c \frac{\Delta^2}{Ut} \right), \quad (66)$$

$$\tilde{M}_s^P = U \left(1 - \lambda'_s \frac{\Delta^2}{Ut} \right). \quad (67)$$

Therefore, contrary to the ionic case, the amplitude of the Peierls distortion is not renormalized to linear order in U and the amplitudes of the relevant scattering processes M_c^P at $U > 0$ and M_s^P at $U < 0$ always increase. Based on this argument one is lead to predict that the deviation from the BI behavior for the attractive ionic Hubbard model and the Peierls-Hubbard model should occur almost at the same values of the on-site interaction. The fundamentally different behaviors of the ionic and the Peierls-Hubbard model will indeed be verified below for repulsive U .

E. The FGN phase diagram

In their paper Fabrizio, Gogolin, and Nersesyan (hereafter FGN) [7] proposed a very challenging scenario of the MI-to-BI crossover in the ionic-Hubbard model on decreasing U at a fixed Δ . The key ingredient of their theory is the existence of *two separate transitions*: a continuous transition at U_{sp}^c where a spin gap is dynamically generated and an Ising type transition at U_{ch}^c where the charge gap vanishes. At $U > U_{sp}^c$ the model exhibits the properties of a MI: the spin excitation spectrum is gapless, charge excitations are gapped, and the vacuum expectation value of the field ϕ_c is locked in one of the degenerate minima $\sqrt{2\pi K_c} \phi_c = \pi \cdot m$ determined only by strong Umklapp scattering. The additive renormalization of the backward scattering amplitude (64) provides the possibility for opening a spin gap at $U < U_{sp}^c$ and one approaches a phase termed by FGN as the spontaneously dimerised insulating (SDI) phase.

The properties of the charge and spin gapped phases as well as the nature of the transition from the BI into the SDI phase, could be quantitatively captured from the following effective potential:

$$\mathcal{V}(\phi_c, \phi_s) = -\tilde{\Delta} \sin\left(\sqrt{2\pi K_c} \phi_c\right) \cos\left(\sqrt{2\pi} \phi_s\right) - \tilde{M}_c \cos\left(\sqrt{8\pi K_c} \phi_c\right) - \tilde{M}_s \cos\left(\sqrt{8\pi} \phi_s\right), \quad (68)$$

where $\tilde{M}_c, \tilde{M}_s, \tilde{\Delta} > 0$ are phenomenological parameters obtained by integrating out high-energy degrees of freedom.

Minimizing $\mathcal{V}(\phi_c, \phi_s)$ with respect to ϕ_c and ϕ_s results in the following sets of vacua:

For $\tilde{\Delta} < 4\tilde{M}_c$ i.e. $U_{ch}^c < U < U_{sp}^c$

$$\begin{aligned} \text{I.} \quad & \sqrt{2\pi} \phi_s = 2\pi n \\ & \sqrt{2\pi K_c} \phi_c = \varphi_0, \quad \pi - \varphi_0 \pmod{2\pi} \\ \text{II.} \quad & \sqrt{2\pi} \phi_s = \pi + 2\pi n \\ & \sqrt{2\pi K_c} \phi_c = -\varphi_0, \quad -\pi + \varphi_0 \pmod{2\pi} \end{aligned} \quad (69)$$

where $\varphi_0 = \arcsin\left(\frac{\tilde{\Delta}}{4\tilde{M}_c}\right)$

while for $\tilde{\Delta} > 4\tilde{M}_c$ i.e. $U < U_{ch}^c$

$$\begin{aligned} \text{I.} \quad & \sqrt{2\pi} \phi_s = 2\pi n \\ & \sqrt{2\pi K_c} \phi_c = \frac{\pi}{2} \pmod{2\pi} \\ \text{II.} \quad & \sqrt{2\pi} \phi_s = \pi + 2\pi n \\ & \sqrt{2\pi K_c} \phi_c = -\frac{\pi}{2} \pmod{2\pi} \end{aligned} \quad (70)$$

and the latter set is easily recognized as the set of vacua corresponding to the BI phase.

Note that the set of vacua in the spin channel (and therefore the spin quantum numbers) does not change within the spin gapped phases at $U < U_{sp}^c$. However the charge sector is strongly different: the existence of two degenerate minima $\varphi_0, \pi - \varphi_0$ at $U_{ch}^c < U < U_{sp}^c$ gives rise to new topological excitations interpolating between the minima of the local double-well potentials. The charge carried by these solitons is

$$Q = 1 - \frac{2\phi_0}{\pi} \quad (71)$$

At $\tilde{\Delta} = 4\tilde{M}_c$ (i.e. $U = U_{ch}^c$) this charge vanishes, while the corresponding mode becomes *gapless*. Since these vacuum-vacuum transitions are intra-set ones, the total spin carried by the zero mode is either $S = 0$ or $S = 1$. Therefore the mode which becomes gapless at $U = U_{ch}^c$ can represent either a spin singlet or a triplet two-particle state. Finally, at $U < U_{ch}^c$ the system shows the properties of the BI.

To clarify the symmetry properties of the various ordered phases we use the following set of order parameters describing the short wavelength fluctuations of the *site*-located charge-density,

$$\Delta_{CDW} \sim \sin(\sqrt{2\pi K_c} \phi_c) \cos(\sqrt{2\pi} \phi_s), \quad (72)$$

the *site*-located spin-density

$$\Delta_{SDW} \sim \cos(\sqrt{2\pi K_c} \phi_c) \sin(\sqrt{2\pi} \phi_s), \quad (73)$$

and the short wavelength fluctuations of the *bond*-located charge- and spin-density

$$\Delta_{Dimer} \sim \cos(\sqrt{2\pi K_c} \phi_c) \cos(\sqrt{2\pi} \phi_s), \quad (74)$$

$$\Delta_{bd-SDW} \sim \sin(\sqrt{2\pi K_c} \phi_c) \sin(\sqrt{2\pi} \phi_s). \quad (75)$$

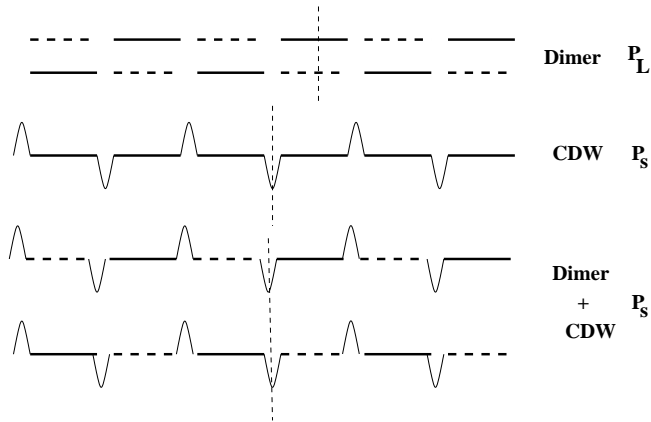


FIG. 2. Illustration of the SDI phase. Top figure: Two degenerate dimerization patterns; the vertical dashed line is a mirror axis indicating the link reflection symmetry of each dimer state. Middle figure: schematic picture for a staggered charge density wave (CDW) which has site reflection symmetry. Lower figure: The superposition of the CDW state with both dimerized patterns again allows for a site reflection symmetric state. This figure serves as a pictorial representation of the SDI state for which the site parity provides a good quantum number.

For $U < U_{ch}^c$ the charge and the spin excitation spectrum are gapped. The vacuum values of the ordered fields are $\langle \phi_s \rangle = 0$ and $\langle \phi_c \rangle = \sqrt{\pi/8K_c}$. Using Eqs. (72)-(75) one obtains the long-range ordered CDW phase

$$\langle \Delta_{CDW}(x)\Delta_{CDW}(x') \rangle \sim const. . \quad (76)$$

For $U_{ch}^c < U < U_{sp}^c$ the vacuum expectation values of the ordered charge field is now different: $\langle \sqrt{2\pi K_c} \phi_c \rangle = \varphi_0$ and still $\langle \phi_s \rangle = 0$. In this phase, the system the long-range ordered CDW and dimer correlations coexist

$$\begin{aligned} \langle \Delta_{CDW}(x)\Delta_{CDW}(x') \rangle &\sim \sin^2 \varphi_0 , \\ \langle \Delta_{BOW}(x)\Delta_{BOW}(x') \rangle &\sim \cos^2 \varphi_0 . \end{aligned}$$

This is the defining property of FGN's SDI phase. We prefer to call it the *CDW + Dimer* phase. The standard dimerized phase violates the site inversion symmetry but preserves the link inversion symmetry. In the *CDW + Dimer* phase, due to the pinning of the CDW by the ionic distortion, the link parity is also broken. However, in the absence of an externally implemented Peierls distortion, the dimer pattern is doubly degenerate as illustrated in Fig. 2. Thus, the charge distribution in the *CDW + Dimer* phase arises as a linear combination of two dimerized patterns with a relative shift by one lattice spacing; in this situation the site inversion symmetry is not broken.

Finally, at $U > U_{sp}^c$ the spin gap disappears. According to FGN, at this point $\varphi_0 = 0$ and the standard MI phase with an identical power-law decay of the SDW and Peierls correlations is realized:

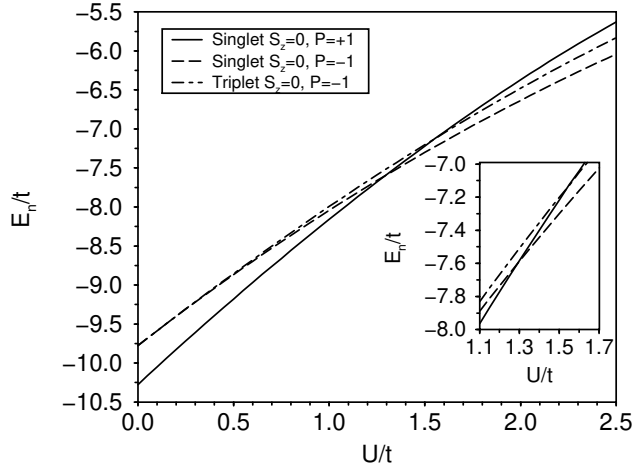


FIG. 3. Lowest energy eigenvalues of the ionic Hubbard model at half filling for $L = 8$ sites, periodic boundary conditions and $\Delta = 0.5t$.

$$\begin{aligned} &\langle \Delta_{Dimer}(x)\Delta_{Dimer}(x') \rangle \\ &\sim \langle \Delta_{SDW}(x)\Delta_{SDW}(x') \rangle \sim \frac{1}{|x-x'|} . \end{aligned} \quad (77)$$

Similar to the standard Hubbard model the CDW ordering is strongly suppressed due to the ordering of the charge field with vacuum expectation value $\langle \phi_c \rangle = 0$.

Below, we present results of our numerical studies of the ground state phase diagram of the one-dimensional ionic-Hubbard model at half filling by exact diagonalization of finite systems with the Lanczos and DMRG methods. From these data we will conclude that the proposed SDI phase is not realized in the ionic Hubbard model.

VII. LANCZOS EXACT DIAGONALIZATION RESULTS

In order to understand the nature of the spectrum and the phase transition, we have diagonalized numerically small systems by the Lanczos method [30]. The energies of the few lowest eigenstates were obtained for finite chains with the number of sites $L = 4n$ and periodic boundary conditions (PBC) or $L = 4n + 2$ with antiperiodic boundary conditions (APBC), for reasons discussed above. The purpose of these calculations is to extend earlier exact diagonalization calculations [14,8] for a better understanding of the symmetries of the eigenstates involved in the level crossing.

We first analyze a short chain without a finite size scaling analysis. The thermodynamic limit will be addressed below by analyzing DMRG results. For chain lengths $L \leq 16$ accessible to exact diagonalization techniques, the finite size effects do not change the qualitative behaviour discussed below. In Fig. 3, the lowest eigenener-

gies of the ionic Hubbard model for $\Delta = 0.5t$, $L = 8$ and PBC are shown as a function of U . At $U = 1.3t$, a level crossing of the two lowest eigenstates occurs signaling a discontinuous phase transition. The level crossing occurs for all chain lengths if the proper boundary conditions are chosen [14,8].

As pointed out before, a non-degenerate eigenstate of the ionic Hubbard model can only have parity eigenvalues ± 1 , so a groundstate level crossing transition corresponds to a change of sign of the parity eigenvalue. In particular, since a state with a spontaneous dimerization, as suggested by Fabrizio *et al.* [7], would have no site inversion symmetry, but the Hamiltonian (1) has, it cannot be a groundstate of (1), except it is degenerate.

For $U = 0$, the Hamiltonian (1) can be easily diagonalized in momentum space, obtaining two energy bands $E_{1/2}(k) = \pm\sqrt{4\cos^2(k) + (\Delta/4)^2}$ with momenta $-\pi/2 < k \leq \pi/2$ restricted to the reduced BZ. This is done by introducing new fermionic creation and annihilation operators $\{\gamma_{k\sigma b}^\dagger, \gamma_{k\sigma b}\}$ with an additional band index $b = 1, 2$ denoting the lower and upper bands, respectively. It is easily verified that the first two degenerate excited states at half filling always have negative site parity, because the ground state has positive parity due to the argument given above, and the operator $\gamma_{q\sigma 2}^\dagger \gamma_{q\sigma 1}$ with $q = \pi/2$ obeys

$$P\gamma_{q\sigma 2}^\dagger \gamma_{q\sigma 1} = -\gamma_{q\sigma 2}^\dagger \gamma_{q\sigma 1}P \quad . \quad (78)$$

The first two excited states shown in Fig. 3 are the spin singlet (total spin $S = 0$, $S_z = 0$, dashed line) and triplet excitations ($S = 1$, $S_z = 0$, dot-dashed line), created from the ground state by applying the operators

$$\begin{aligned} & \frac{1}{\sqrt{2}} \left(\gamma_{q\uparrow 2}^\dagger \gamma_{q\uparrow 1} - \gamma_{q\downarrow 2}^\dagger \gamma_{q\downarrow 1} \right) , \\ & \frac{1}{\sqrt{2}} \left(\gamma_{q\uparrow 2}^\dagger \gamma_{q\uparrow 1} + \gamma_{q\downarrow 2}^\dagger \gamma_{q\downarrow 1} \right) , \end{aligned} \quad (79)$$

respectively. Thus, both excited states have total momentum $k_{tot} = 0$ and negative site parity. For $U > 0$, these degenerate states split in energy.

Fig. 4 shows the overlap matrix elements between the exact ground states $|\psi_0\rangle = |U/t, \Delta/t, \delta/t\rangle$ of the ionic Hubbard model ($\Delta = 0.5t$, $\delta = 0$), the Peierls-Hubbard model ($\Delta = 0$, $\delta = 0.5t$), and the ordinary Hubbard model ($\Delta = \delta = 0$). In the upper figure, the overlaps $\langle U, 0.5, 0 | 0, 0.5, 0 \rangle$ between the ground states of the ionic Hubbard model for $0 < U < 2.9t$ and $U = 0$ (black circles), and $\langle U, 0.5, 0 | 2.9, 0.5, 0 \rangle$ for the ground states of the ionic Hubbard model for $0 < U < 2.9t$ with and $U = 2.9t$ (white circles) are shown. Clearly, there occurs a sharp transition at $U_C = 1.5t$, with the ground states $|U, 0.5, 0\rangle$ for $U < U_C$ and $U > U_C$ being orthogonal to each other. In contrast, within the same phase the ground state changes weakly but continuously with U . This reflects the level crossing phenomenon, where two orthogonal states cross, that differ at least in one quantum number, which is

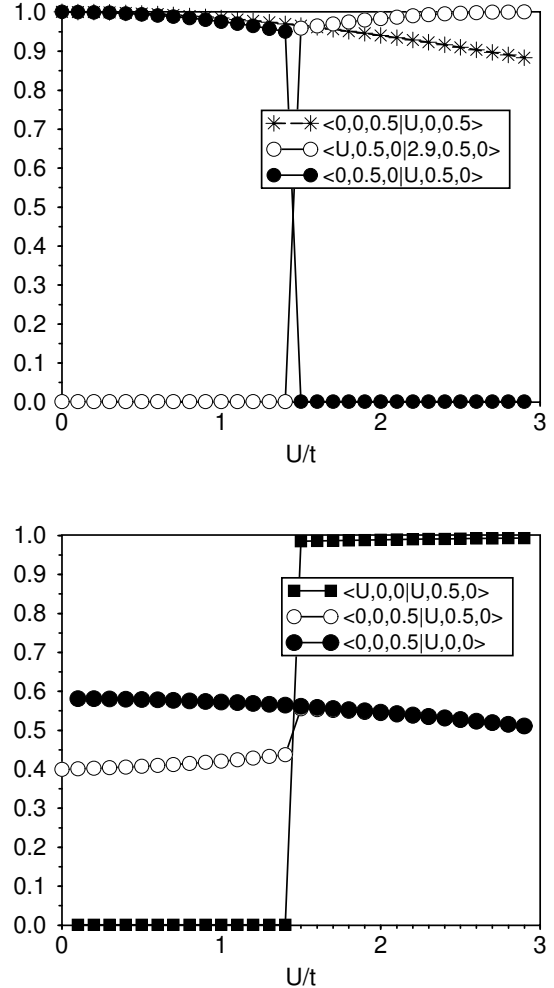


FIG. 4. Various overlap matrix elements of the exact diagonalization ground states $|\psi_0\rangle = |U/t, \Delta/t, \delta/t\rangle$ of the ionic Hubbard model ($\Delta = 0.5t$, $\delta = 0$), the Peierls-Hubbard model ($\Delta = 0$, $\delta = 0.5t$), the ordinary Hubbard model ($\Delta = \delta = 0$), and the Peierls chain ($U = \Delta = 0$) as a function of U . For details see the text and the legends in the figures. Calculations were performed for $L = 10$ sites, half filling, and with antiperiodic boundary conditions.

the site parity. In case of the Peierls-Hubbard model ($\Delta = 0$, $\delta = 0.5t$), the situation is different. The overlap $\langle 0, 0, 0.5 | U, 0, 0.5 \rangle$ between the ground states for $U = 0$ and $U > 0$ (black stars) decreases slowly and continuously with increasing U , and no indication of a phase transition is observed. Thus, this model is a BI only at $U = 0$, and turns into a correlated Peierls insulator for any infinitesimal $U > 0$.

The lower figure illustrates the relation between the different models. It shows the overlap $\langle U, 0, 0 | U, 0.5, 0 \rangle$ between the ground states of the ordinary and the ionic Hubbard models for a given value of U . Below U_C , the

VIII. DMRG RESULTS

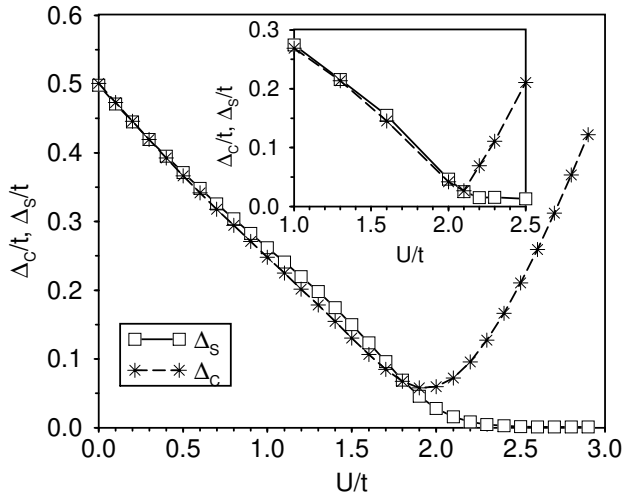


FIG. 5. Results for the spin (Δ_S) and charge (Δ_C) gap of the 1D ionic Hubbard model at half-filling with an on-site energy modulation $\Delta = 0.5t$ as a function of the on-site Coulomb repulsion U . Energies were obtained by DMRG calculations on open chains with $L = \{30, 40, 50, 60\}$ (main plot) and $L = \{30, 40, 50, 60, 200, 300\}$ (inset), and extrapolated to the infinite chain length limit.

ground state for $\Delta > 0$ has site parity $+1$ and thus is orthogonal to the one for $\Delta = 0$ (which has site parity -1), whereas for $U > U_C$ the ground state of the ionic model is very close to the one of the ordinary Hubbard model (both having site parity -1), with a small deviation reflecting the different charge distributions (staggered versus homogeneous).

In addition, the groundstate overlaps of the ionic and the ordinary Hubbard model with a Peierls chain of free fermions ($\Delta = 0, U = 0$) are plotted. Again, for $U > U_C$ the two models appear to be quite similar with respect to the location of electrons on the bonds (measured by the overlap with a dimerized chain), whereas for $U < U_C$ the ionic model appears quite different, because for $\Delta > 0$ the electrons prefer to stay in the potential wells of the odd sites.

Obviously, from symmetry considerations and exact diagonalizations of finite rings already a quite clear picture of the phase diagram of the model emerges. At a finite $U_C > 0$, a level crossing phase transition occurs, connected with a change of parity of the ground state. It separates two phases, a band insulator at $U < U_C$ and a correlated insulator with a finite staggered charge modulation for all values of $U > U_C$.

To check whether the scenario emerging from symmetry considerations and exact diagonalizations of small rings holds for the thermodynamic limit, we have calculated Δ_C and Δ_S for longer chains using the DMRG method [31,32]. In Fig. 5 extrapolated results for Δ_C and Δ_S are shown as a function of U . Calculations were performed with open boundary conditions (OBC) for chains of lengths $L = \{30, 40, 50, 60\}$ for all selected values of U , and additionally for $L = 200$ and $L = 300$ in the transition region around the estimated U_C . Note that in contrast to the definition (2), the charge gap was obtained in the DMRG calculations using

$$\Delta_C = \frac{1}{2} \left[E_0(N = L + 2, S_z = 0) + E_0(N = L - 2, S_z = 0) - 2E_0(N = L, S_z = 0) \right] \quad (80)$$

in order to calculate the relevant energies E_0 remaining in the subspace $S_z = 0$. This becomes equivalent with (2) in the thermodynamic limit. We assume the scaling behavior of Δ_C and Δ_S with the chain length L to be of the form [33]

$$\Delta_i(L) = \Delta_i^\infty + \frac{A_i}{L} + \frac{B_i}{L^2} + \dots, \quad (81)$$

where $i \in \{S, C\}$. This scaling behaviour is the usual choice used for finite size extrapolations of data obtained with OBC. Extrapolation to the infinite chain length limit is then done by fitting this polynomial in $1/L$ to the calculated finite chain results. We note that different finite size scaling formulas were proposed in the literature mainly when PBC or APBC were used. For example, Gidopoulos *et al.* [8] use

$$\Delta_i(L) = \sqrt{(\Delta_i^\infty)^2 + \frac{A_i}{L^2} + \frac{B_i}{L^3} + \dots} \quad (82)$$

to extrapolate their exact diagonalization results. For the spin gap Δ_S a frequently used ansatz for the scaling behaviour is of the form [34]

$$\Delta_S(L) = \Delta_S^\infty + \frac{A}{L^p} e^{-L/L_0}, \quad (83)$$

which incorporates a power law in $1/L$ times an exponential involving a characteristic length scale L_0 .

The fact that the transition at U_C is connected with inversion symmetry requires some caution when open boundary conditions are used. It is obvious that in this case for $L = 2n$ the Hamiltonian (1) is not reflection symmetric at any site. Thus, the ground state of a finite size chain with open boundary conditions does not have

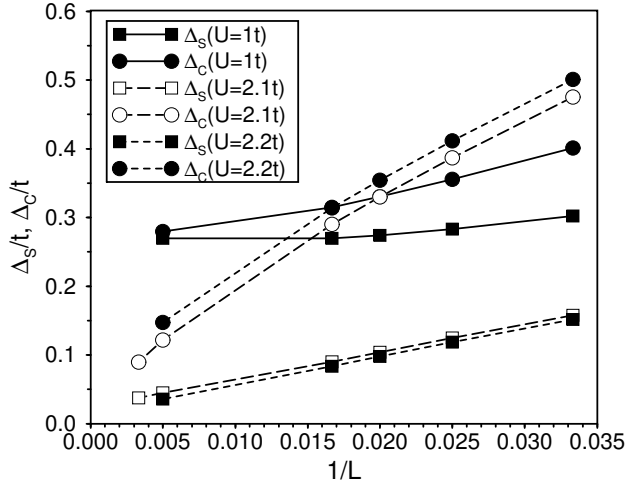


FIG. 6. Chain length dependence of the DMRG results for the spin (Δ_S) and charge (Δ_C) gap of the half-filled 1D ionic Hubbard model with an on-site energy modulation $\Delta = 0.5t$ for selected values of the on-site Coulomb repulsion U .

a well defined site parity, and the level crossing transition does not occur in such a system. Instead, only a smooth crossover is observed. To overcome this problem, one might try to use chains with OBC and an *odd* number of sites $L = 2n + 1$, since the Hamiltonian in this case is reflection symmetric with respect to the site i_c in the center of the chain, and a site parity operator is well defined by

$$P c_{i_c \sigma}^\dagger P^\dagger = c_{L-1-i_c \sigma}^\dagger . \quad (84)$$

To check whether this is an improved choice we have calculated the site parity of the ground state for $U = 0$ analytically for different chain lengths $L = 2n + 1$. We found that the site parity eigenvalue of the $U = 0$ ground state is

$$P|\psi_0\rangle = (-1)^n |\psi_0\rangle . \quad (85)$$

On the other hand, in the large U limit ($U \gg t$) again the mapping to the Heisenberg Hamiltonian could be used to obtain the site parity eigenvalue. By extending the idea of Gidopoulos *et al.* [8] to chains with $L = 2n + 1$, for $U \gg t$ we obtain

$$P|\psi_0\rangle = (-1)^{\sum_{m=1}^{L-1} m} |\psi_0\rangle = (-1)^n |\psi_0\rangle . \quad (86)$$

Thus, the parity eigenvalue of the ground state is the same at $U = 0$ and $U \gg t$ for a given chain length, and no level crossing occurs. As mentioned above, the argument for $U \gg t$ requires some caution, so we also have checked this result numerically by exact diagonalizations of small systems with $L = 5, 7, 9, \dots$. Indeed, no level

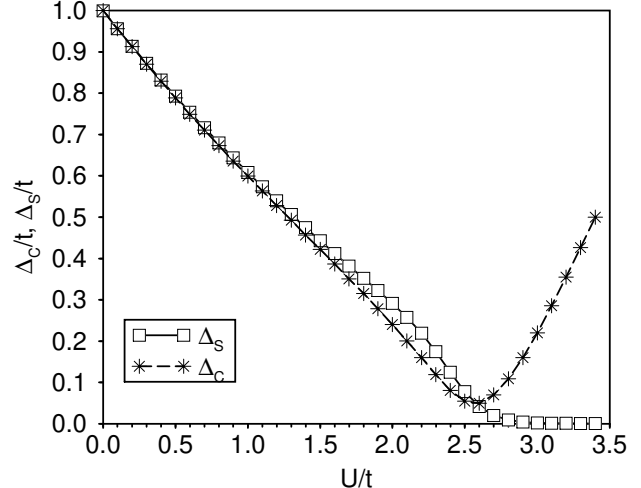


FIG. 7. Same as Fig. 4, but for an on-site energy modulation $\Delta = 1t$. The ground state energies were obtained with $L = \{30, 40, 50, 60\}$ and extrapolated to the thermodynamic limit.

crossing was observed. Thus we conclude that also for odd numbers of sites and OBC the level crossing in the ground state does not occur.

Obviously, results for any choice of boundary conditions should recover the level crossing scenario when extrapolated to the thermodynamic limit. Due to the fact that the sharp transition at a well defined U_C does not exist in the finite chain results for OBC, the extrapolation is a quite subtle problem, since a sharp transition feature has to be identified from the extrapolation of smooth curves. This requires the use of quite long chains in the critical region (up to at least $L = 300$ sites).

As can be seen from the main plot in Fig. 5, extrapolating the results for $L = \{30, 40, 50, 60\}$ does not give a sharp transition behaviour of the gaps. Up to approximately $U \sim 0.4t$, the band insulator with $\Delta_C = \Delta_S$ persists, and for $U > 2.3t$ the system is a correlated insulator with $\Delta_C > 0$ and $\Delta_S < \Delta_C$. Within numerical accuracy $\Delta_S = 0$, which suggests that this phase represents a true MI. However, the possibility remains, that Δ_S is only very small but finite. This question cannot be finally answered by numeric results. The intermediate region does not show a clear sharp transition, the charge gap never closes, and one observes $\Delta_C \neq \Delta_S$ already below the estimated U_C .

As illustrated in the inset of Fig. 5, adding results for $L = 200$ and even $L = 300$ in the critical region changes the picture considerably, approaching the behaviour expected from symmetry considerations and exact diagonalization results. This allows the conclusion that the above level crossing scenario will be recovered in the thermodynamic limit for the DMRG results on chains with an

$U = 1t$				
L	$E_0(L, 0)$	$E_0(L, 1)$	$E_0(L + 2, 0)$	$E_0(L - 2, 0)$
30	-31.232	-30.930	-29.831	-31.831
40	-41.873	-41.590	-40.517	-42.517
50	-52.515	-52.241	-51.185	-53.185
60	-63.157	-62.888	-61.843	-63.843
200	-212.153	-211.883	-210.870	-212.878

$U = 2.2t$				
L	$E_0(L, 0)$	$E_0(L, 1)$	$E_0(L + 2, 0)$	$E_0(L - 2, 0)$
30	-24.099	-23.948	-21.398	-25.798
40	-32.308	-32.190	-29.697	-34.097
50	-40.518	-40.420	-37.964	-42.364
60	-48.728	-48.644	-46.214	-50.614
200	-163.672	-163.636	-161.324	-165.725

TABLE I. Ground state energies $E_0(N, S_z)$ for selected values of U and different particle numbers N , total spin z -components S_z , and chain lengths L , as obtained by our DMRG calculations.

even number of sites. To illustrate the dependence of the gaps on the chain lengths L , a scaling plot for Δ_C and Δ_S at selected values of U is shown in Fig. 6. The changes in the behaviour occurring for longer chains are clearly visible. In Table I, ground state energies $E_0(N, S_z)$, from which the gaps in Fig. 6 were calculated, are given for two selected values of U . The DMRG calculations were performed with four finite lattice sweeps, and the number of states kept in the DMRG projection was increased from $m = 100$ to $m = 300$ during the sweeps.

Our results are in general agreement with the DMRG results obtained by Qin *et al.* [23]. These authors performed DMRG calculations for the ionic Hubbard model with $\Delta = 0.6t$, obtaining Δ_S and Δ_C for chains up to $L = 600$ sites with a maximum of $m = 500$ states kept in the DMRG projection. In contrast to our calculations, Qin *et al.* used the definition (2) to calculate the charge gaps. They performed a finite size analysis assuming the same polynomial dependence (81) of Δ_S and Δ_C on $1/L$. Surprisingly, they observed a non-monotonic scaling behaviour of Δ_S with L for values of U close to the critical U_C , i.e. for chain lengths $L > 300$ Δ_S started to increase again. It remains unclear whether this is due to losing DMRG accuracy with increasing chain lengths, or indicates that an intrinsic length scale is appearing for the spin degrees of freedom.

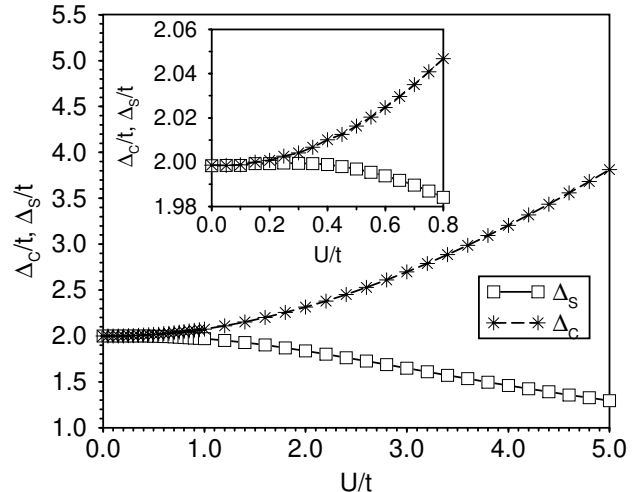


FIG. 8. Results for the spin (Δ_S) and charge (Δ_C) gap of the Peierls-Hubbard model at half-filling with a modulation of the hopping amplitude $\delta = 0.1t$ as a function of the on-site Coulomb repulsion U . Energies were obtained by DMRG calculations on open chains with $L = \{30, 40, 50, 60\}$.

Similar DMRG calculations for the ionic Hubbard model with $\Delta = 1t$ have also been performed by Takada and Kido [22] for chains up to $L = 400$ sites, using also the relation (81) for the finite size extrapolation. The data presented in [22] seem to be in agreement with our results. However, the authors interpret the intermediate region close to U_C in favour of a two-transition-scenario similar to that of Fabrizio *et al.* [7]. In Fig. 7 our extrapolated results for a larger $\Delta = 1t$ are shown, corresponding to the parameters used in Ref. [22]. These data were again obtained for chains $L = \{30, 40, 50, 60\}$, so only the smooth crossover is seen. But it illustrates how the transition shifts to higher values of U for increasing Δ .

It becomes obvious from this discussion, that DMRG studies requiring OBC can face problems when the transition under consideration is connected with a change in spatial symmetries broken by the OBC. Closed boundary conditions in such a system describe the infinite chain much better than open ones, but suffer from the commonly observed reduced DMRG accuracy for closed chains.

For comparison we show in Fig. 8 the spin and charge gaps versus U in the Peierls-Hubbard model ($\Delta = 0$, $\delta > 0$). As already anticipated in previous chapters this model does not show any signature for a phase transition; i.e. $\Delta_c > \Delta_s > 0$ for any value of the interaction $U > 0$. So although the Peierls and the ionic insulator for $U = 0$ similarly open an excitation gap at the zone boundary due to the doubling of the unit cell, switching on the Coulomb U leads to distinct in both cases. The origin

of the different behaviors must be traced to the fact that the Hubbard interaction and the ionic potential compete locally on each site while the Peierls modulation of the hopping amplitude tends to concentrate electronic charge on the bonds between sites thereby avoiding conflict with the Hubbard term. This difference is reflected in the important different structures of the ionic and the Peierls term in the bosonized versions of the Hamiltonian (see chapter VI).

IX. OPTICAL CONDUCTIVITY

To further analyze the band and correlated insulating phases below and above U_C , we have calculated the frequency-dependent optical conductivity within the dynamical DMRG (DDMRG) approach making use of the very accurate correction vector technique described in [36]. Calculations were performed for $L = 128$ sites with OBC using a Parzen filter to suppress the influence of the chain boundaries, as proposed in [36].

The real part of the longitudinal optical conductivity $\sigma(\omega)$ is determined by the linear response of the system to an external electromagnetic field. In the Kubo formalism, $\sigma(\omega)$ is connected to the imaginary part of the retarded current-current correlation function

$$\begin{aligned} \chi_{jj}(q, \omega) &= \frac{i}{La} \int_0^\infty d\tau e^{i\omega\tau} \langle \psi_0 | [j_{-q}(\tau), j_q(0)] | \psi_0 \rangle \\ &= \frac{\hbar}{La} \sum_{n \neq 0} \left(\frac{|\langle \psi_n | j_q | \psi_0 \rangle|^2}{\hbar\omega + (E_n - E_0) + i0^+} \right. \\ &\quad \left. - \frac{|\langle \psi_n | j_q | \psi_0 \rangle|^2}{\hbar\omega - (E_n - E_0) + i0^+} \right) \quad , \quad (87) \end{aligned}$$

with τ the time index, a the distance between neighboring sites, and $|\psi_n\rangle$ and E_n ($n = 0, 1, 2, \dots$) denoting the eigenstates and the respective energies. Thus, for $\omega > 0$ the imaginary part of $\chi_{jj}(q, \omega)$ can be obtained numerically from [38]

$$\begin{aligned} \text{Im} \chi_{jj}(q, \omega) &= \quad (88) \\ -\frac{\hbar}{La} \text{Im} \langle \psi_0 | j_q \frac{1}{\hbar\omega + E_0 - H + i0^+} j_q | \psi_0 \rangle \quad . \end{aligned}$$

Here, the paramagnetic current operator is defined by

$$j_q = -it \frac{ea}{\hbar} \sum_{i, \sigma} e^{iqx_i} \left(c_{i+1\sigma}^\dagger c_{i\sigma} - c_{i\sigma}^\dagger c_{i+1\sigma} \right) \quad , \quad (89)$$

where e is the electron charge. The real part of the optical conductivity in the long wavelength limit $q = 0$ is then given by

$$\sigma_1(\omega) = D\delta(\omega) + \sigma_1^{reg}(\omega > 0) \quad (90)$$

$$\sigma_1^{reg}(\omega > 0) = \frac{1}{\hbar\omega} \text{Im} \chi_{jj}(q = 0, \omega) \quad . \quad (91)$$

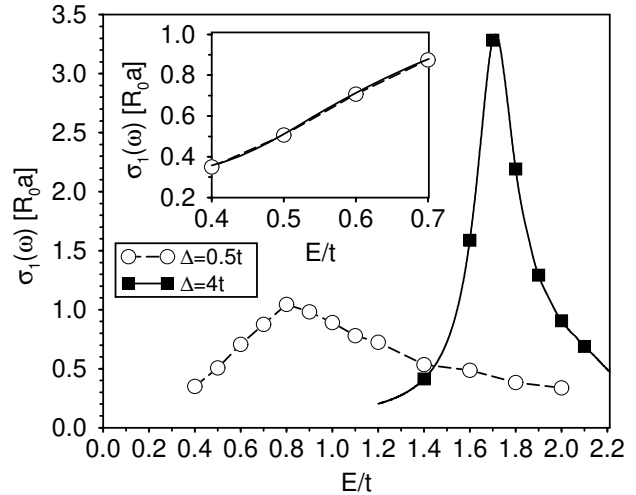


FIG. 9. Real part of the optical conductivity $\sigma_1(\omega)$ in units of $R_0 a = e^2 a / \hbar$ vs. energy $E = \hbar\omega$ for the half-filled 1D ionic Hubbard model for $U = 3t$. The results have been obtained by DDMRG calculations using the correction vector method for a chain with $L = 128$ sites and open boundary conditions. A finite broadening $\eta = 0.1t$ of the peaks has been used. The selected values of the on-site modulation Δ correspond to the BI ($\Delta = 4t$) and the correlated insulator ($\Delta = 0.5t$). The inset shows a fit (solid black line) to the onset region of $\sigma_1(\omega)$ above the charge gap in the correlated insulator (see text).

For the insulating phases of the ionic Hubbard model at half-filling the Drude weight vanishes $D = 0$, so that $\sigma_1(\omega) = \sigma_1^{reg}(\omega)$.

In the absence of interactions $U = 0$, the conductivity vanishes below the band gap Δ , and diverges as $\sigma_1(\omega) \sim \frac{1}{\sqrt{\omega - \Delta}}$ for $\omega \rightarrow \Delta$ and $\omega > \Delta$ [37]. We expect this behavior to persist upon increasing U over the entire BI phase. This implies that the physics of the excitations in the BI phase remains similar for $0 \leq U < U_C$. In order to test the validity of this scenario, we have evaluated the optical conductivity in the BI phase by DDMRG [36]. For the correction vector method a separate DMRG run has to be performed for each selected frequency ω . In Fig. 9, the DDMRG results for a chain with $L = 128$ sites and OBC are plotted for $U = 3t$. For the proper convergence of the correction vector algorithm a finite broadening $\eta = 0.1t$ in Eq. (89) was chosen. For $\Delta = 4t$, the solid black line interpolating between the discrete data points at different frequencies was calculated by additionally applying the Lanczos vector method after the DMRG sweeps, obtaining the correlation function also in the vicinity of the selected frequencies [36]. The results presented in Fig. 9 support the previous interpretation. One observes a dominant low energy excitation peak above the optical gap at around $E \approx 1.7t$. The Lorentzian tail for $E < 1.7t$ results from the necessarily

large broadening $\eta = 0.1t$. Also, in the correction vector results the square root divergence for $\hbar\omega \rightarrow \Delta$ is not visible due to the finite size of the system. However, it is anticipated by the dominant excitation peak in the finite size results.

For $U > U_C$, the situation is different, as demonstrated in Fig. 9 as well. There we show $\sigma_1(\omega)$ for $U = 3t$ and $\Delta = 0.5t$ with the same broadening $\eta = 0.1t$ and $L = 128$ for OBC. The dashed line connecting the data points (white circles) serves only as a guide to the eye. In the correlated insulator phase, at least the behavior of the charge excitations, is expected to be similar to that in the normal ($\Delta = 0$) repulsive Hubbard model, where it is known that $\sigma_1(\omega)$ behaves like $\sigma_1(\omega) \sim \sqrt{\omega - \Delta_C}$ above the charge gap Δ_C . This was also demonstrated recently by DDMRG calculations [38]. In the inset of Fig. 9, $\sigma_1(\omega)$ is plotted on a finer energy scale in the onset region above the gap Δ_C . The solid black line is a fit to the DDMRG data obtained by convoluting $\sqrt{\hbar\omega - \Delta_C}$ with a Lorentzian of width η , i.e. by using the fit formula

$$\sigma_1(\omega) = \frac{A}{\hbar\omega\pi} \int_{\Delta_C}^{\nu_{max}} dv \frac{\eta\sqrt{\nu - \Delta_C}}{(\nu - \hbar\omega)^2 + \eta^2} \quad , \quad (92)$$

where A is an adjustable prefactor and ν_{max} the upper bound for the square root dependence. The fit in Fig. 9 has been obtained using the parameter values $A = 1.9t$, $\nu_{max} = 1.5t$, and $\Delta_C = 0.48t$. The value for Δ_C is consistent with the charge gaps presented in Fig. 5. The agreement between this fit and the DDMRG results is quite striking. Thus, one can safely conclude that the numerical results are in agreement with the behavior expected for a correlated (Mott) insulator in 1D. The qualitative behavior of $\sigma_1(\omega)$ is also in agreement with the results obtained for the normal Hubbard model at $U = 3t$ [38]. Thus, it is concluded that the physics of the charge excitations above U_C compares well to that of the Hubbard chain for $\Delta = 0$.

Whenever the site parity is well defined for the ground state, i.e. in the thermodynamic limit, and for finite systems with the appropriate boundary conditions, the current operator $j_{q=0}$ changes the parity when acting on that state. Thus, the matrix elements $\langle \psi_n | j_{q=0} | \psi_0 \rangle$ in (87) vanish for all states with $P|\psi_n\rangle = P|\psi_0\rangle$, i.e. it connects the ground state only to states with opposite site parity eigenvalues. In the ionic Hubbard model, the first two excited states have opposite parity with respect to the ground state, as was demonstrated in Fig. 3, and the corresponding singlet state which determines the charge excitation gap therefore also contributes to the optical conductivity.

Precisely at the critical U_C , the ground state and the first excited state cross, i.e. $E_1 = E_0$, so the ground state is degenerate and the matrix element $\langle \psi_1 | j_{q=0} | \psi_0 \rangle$ between these states remains finite due to their different site parity eigenvalues. Therefore, the optical gap vanishes at U_C implying the existence of optical excitations

at arbitrary small energies $\omega > 0$. For this reason the critical point has been commonly referred to in the literature as “metallic”. However, by definition a metal is characterized not only by gapless excitations, but also by a finite Drude weight $D > 0$. But due to the ground state degeneracy the Drude weight D for $U = U_C$ is not properly defined. Thus, it follows that the ionic Hubbard model for $U = U_C$ has a gapless optical spectrum, but it cannot be considered “metallic” in the usual sense. (Following the definition of W. Kohn a metal has a finite Drude weight $D > 0$ [39].)

X. CONCLUSIONS

We believe that our combined analytical and numerical analysis clarifies and establishes the ground state structure of the ionic Hubbard model. A single transition at a critical $U_C(\Delta)$ separates a band insulator from a Mott insulator phase. The transition is of the level crossing type, i.e. first order, and connected to a site parity change of the ground state. The previously suggested intermediate SDI phase is not realized. The ionic Hubbard model is also distinctly different from the Peierls-Hubbard model for which the spin and charge excitation gaps are always finite and $\Delta_C = \Delta_S$ for all U and δ . At the critical metallic line $U_C(\Delta)$ the charge gap vanishes and our dynamical DMRG data for the optical conductivity suggest that the square root onset of $\sigma_1(\omega)$ at the optical gap in the Mott insulator phase changes to an inverse square root singularity onset in the band insulator phase.

The existence of an insulator-insulator transition in the 1D ionic Hubbard model at half-filling naturally raises the question whether a ground state phase transition finds its continuation also when the system is doped away from half-filling. The possible consequences for the dynamics of the doped charge carriers and the phenomenon of spin-charge separation will be the topic of future investigations of the ionic Hubbard model.

ACKNOWLEDGMENTS

It is a pleasure to thank M. Fabrizio and A. Nersisyan for fruitful discussions and R. Noack for instructive comments on the DMRG method. This work was supported by the Deutsche Forschungsgemeinschaft (DFG) through Schwerpunkt 1073. APK also acknowledges support through Sonderforschungsbereich 484 of the DFG. GIJ also acknowledges support by the INTAS-Georgia grant N 97-1340.

- [1] For a review see: M. Imada, A. Fujimori, and Y. Tokura, *Rev. Mod. Phys.* **70**, 1039 (1998).
- [2] D. H. Lee and R. Shankar, *Phys. Rev. Lett.* **65**, 1490 (1990).
- [3] C. Aebischer, D. Baeriswyl, and R. M. Noack, *Phys. Rev. Lett.* **86**, 468 (2001).
- [4] J. Sólyom, *Adv. Phys.* **28**, 201 (1979); J. Voit, *Rep. Prog. Phys.* **57**, 977 (1995).
- [5] J. B. Torrance *et al.*, *Phys. Rev. Lett.* **46**, 253 (1981); *ibid.* **47**, 1747 (1981).
- [6] N. Nagaosa and J. Takimoto, *J. Phys. Soc. Jpn.* **55**, 2735 (1986); N. Nagaosa, *ibid.* **55**, 2754 (1986).
- [7] M. Fabrizio, A. O. Gogolin, and A. A. Nersesyan, *Phys. Rev. Lett.* **83**, 2014 (1999); *Nucl. Phys. B* **580**, 647 (2000).
- [8] N. Gidopoulos, S. Sorella, and E. Tosatti, *Eur. Phys. J. B* **14**, 217 (2000).
- [9] T. Mitani *et al.*, *Phys. Rev. Lett.* **53**, 842 (1984); Y. Tokura *et al.*, *Sol. State Comm.* **43**, 757 (1982); *Mol. Cryst. Liq. Cryst.* **125**, 71 (1985); T. Mitani *et al.*, *Phys. Rev. B* **35**, 427 (1987); K. Takaoka *et al.*, *ibid.* **36**, 3884 (1987); Y. Tokura *et al.*, *ibid.* **38**, 2215 (1988).
- [10] M. LeCointe *et al.*, *Phys. Rev. B* **51**, 3374 (1995).
- [11] A. Girlando and A. Painelli, *Phys. Rev. B* **34**, 2131 (1986).
- [12] T. Egami, S. Ishihara, and M. Tachiki, *Science* **261**, 1307 (1993).
- [13] S. Ishihara, T. Egami, and M. Tachiki, *Phys. Rev. B* **49**, 8944 (1994).
- [14] R. Resta and S. Sorella, *Phys. Rev. Lett.* **74**, 4738 (1995).
- [15] R. E. Cohen and H. Krakauer, *Phys. Rev. B* **42**, 6416 (1990).
- [16] L. T. Hudson, *Phys. Rev. B* **47**, 1174 (1993).
- [17] T. Neumann *et al.*, *Phys. Rev. B* **46**, 10623 (1992).
- [18] J. Zak, *Phys. Rev. Lett.* **62**, 2747 (1989).
- [19] R. Resta, M. Posternak, and A. Baldereschi, *Phys. Rev. Lett.* **70**, 1010 (1993).
- [20] G. Ortiz, P. Ordejón, R. M. Martin, and G. Chiappe, *Phys. Rev. B* **54**, 13515 (1996).
- [21] R. Resta, *Phys. Rev. Lett.* **80**, 1800 (1998).
- [22] Y. Takada and M. Kido, *J. Phys. Soc. Jpn.* **70**, 21 (2001).
- [23] S. Qin *et al.*, preprint cond-mat/0004162, unpublished.
- [24] T. Wilkens and R. M. Martin, *Phys. Rev. B* **63**, 235108 (2001).
- [25] Y. Anusooya-Pati, Z. G. Soos, and A. Painelli, *Phys. Rev. B* **63**, 205118 (2001).
- [26] A. H. MacDonald, S. M. Girvin, and D. Yoshioka, *Phys. Rev. B* **37**, 9753 (1988).
- [27] M. Takahashi, *J. Phys. C* **10**, 1289 (1977).
- [28] F. D. M. Haldane, *Phys. Rev. B* **25**, 4925 (1982); K. Okamoto and K. Nomura, *Phys. Lett. A* **169**, 433 (1993); G. Castilla, S. Chakravarty, and V. J. Emery, *Phys. Rev. Lett.* **75**, 1823 (1995).
- [29] For a review see A. O. Gogolin, A. A. Nersesyan, and A. M. Tsvelik, *Bosonization and strongly correlated systems*, Cambridge University Press (1998).
- [30] C. Lanczos, *J. Res. Natl. Bur. Stand.* **45**, 255 (1950).
- [31] S. R. White, *Phys. Rev. Lett.* **69**, 2863 (1992); *Phys. Rev. B* **48**, 10345 (1993).
- [32] I. Peschel, X. Wang, M. Kaulke, K. Hallberg (Eds.): *Density-Matrix Renormalization*, Springer (1999).
- [33] R. Noack, private communication.
- [34] T. Barnes, E. Dagotto, J. Riera, and E. S. Swanson, *Phys. Rev. B* **47**, 3196 (1993).
- [35] K. A. Hallberg, *Phys. Rev. B* **52**, R9827 (1995).
- [36] T. D. Kühner and S. R. White, *Phys. Rev. B* **60**, 335 (1999).
- [37] F. Gebhard, K. Bott, M. Scheidler, P. Thomas, and S. W. Koch, *Phil. Mag. B* **75**, 1 (1997).
- [38] E. Jeckelmann, F. Gebhard, and F. H. L. Essler, *Phys. Rev. Lett.* **85**, 3910 (2000).
- [39] W. Kohn, *Phys. Rev.* **133**, A171 (1964).